Experimental Determination of the Aerodynamic Characteristics and Flap Hinge Moment of the Wing Airfoil used at ITA's Unmanned Aerial Vehicle (UAV)

André Valdetaro Gomes Cavalieri
Instituto Tecnológico de Aeronáutica (ITA). Praça Mal. Eduardo Gomes, 50, S J Campos – SP, Brasil
andre@ita.br

Roberto da Mota Girardi
Instituto Tecnológico de Aeronáutica (ITA). Praça Mal. Eduardo Gomes, 50, S J Campos – SP, Brasil
girardi@ita.br

Tiago Barbosa de Araújo
Instituto Tecnológico de Aeronáutica (ITA). Praça Mal. Eduardo Gomes, 50, S J Campos – SP, Brasil
araujotb@ita.br

Abstract. *The UAV considered in this work has the specific mission of examining elements of an electric energy transmission line (the tower, vegetation at the neighbor area and the electric cables). Such aircraft has some particular characteristics: (i) a relatively small velocity, that is, low Reynolds number, (ii) different material and manufacturing techniques are used and (iii) the weight is very low and, therefore, the aircraft will be very sensitive to atmospheric gusts. Such characteristic increases the difficulty to accomplish the mission, that is, performing a pre-defined path along a transmission line and its elements imaging. The present work objective is to obtain the aerodynamic characteristic curves (CL x α, CL x Cm e CL x CD) of the airfoils chosen to be used at the wing, horizontal and vertical tail of the aircraft being developed. The experimental work will be performed at the ITA wind tunnel and the results will be correct to consider the wind tunnel walls interference. Numerical results will be compared with experimental ones in order to perform a calibration of the numerical tool for the specific Reynolds number considered. Such calibration will be very useful because airfoil can be changed in more advanced design phases.*

Keywords*: Unmanned Aerial Vehicle, Airfoil, Experimental Method, Blockage effect, Numerical Solution*

1. INTRODUCTION

Unmanned aerial vehicles (UAV) can be used in several civil applications, like that: (i) Electrical lines and pipelines examination, (ii) harbors, forest reservations and less accessible frontiers vigilance, (iii) aircraft and disappeared people rescue, (iv) aerial picture generation and (v) others.

In 2004 Technological Institute of Aeronautics (ITA) was contacted to participate in a cooperation involving Advanced System Studies Center of Recife (CESAR) and São Francisco Electric Company (CHESF). The goal of such cooperation was an UAV development, for electrical line elements (towers, vegetation existing in the neighborhood of electrical lines, electrical connectors at the towers and etc) examination. In order to accomplish this task, a very low velocity (80 km/h) aircraft, flying at low altitude, is required, due to infrared camera limitations (required to observe hot spots, which indicate electric problems at some line elements). In such velocity range, atmospheric gusts became very important due to these effects on the flight security and because the electric line elements examination mission became very difficult, due the constant aircraft attitude changes.

The low aircraft velocity, required to accomplish the infrared camera examination mission, is in the inferior limit of an airplane flight envelope, because a high wing loading (W/S) is necessary to give the aircraft a low sensibility to atmospheric gusts, but, on the other hand, a low value of W/S is required to accomplish the low velocity flight requirement. All mission requirements could be fulfilled by using other kinds of aircrafts, like a helicopter, a dirigible or a hybrid vehicle, that is, a mixture between a dirigible and an airplane, for example. The most adapted kind of aircraft was analyzed by Girardi and Rizzi (2005a), where an airplane was chosen to be the kind of aircraft used in this project.

The second step in the conceptual phase of the airplane project was the definition of the more adapted configuration, considering all requirements fulfillment. Two basic airplane configurations were considered: (i) in the first one the engine is located at the airplane nose, a conventional tail was chosen to give stability and control to the aircraft and the camera was located at the fuselage low surface, near the aircraft gravity center (GC). (ii) In the second configuration, the engine was located at the fuselage tail, in the pusher configuration, and two booms were used to assembly the tail to the wing. In this configuration, the camera could be located at the fuselage nose or in the same place of the first configuration. Both configurations have high wing position (relative to the fuselage), a tricycle landing gear type and a rectangular wing. These configurations were analyzed by Girardi and Rizzi, (2005b) and the first one was chosen, considering the camera position near the aircraft GC (better to decrease effects on the camera due to the aircraft constant attitude changes, associated to the gusts effects) and the design team experience.

The aircraft conceptual design phase was executed by the Aeronautics Department of ITA and a special methodology was developed (Girardi e Rizzi, 2006) to face the problems associated to the airplane specific mission, that is, image acquisition from an aircraft at low velocity, manufactured with non conventional material and subjected to atmospheric gusts, because of the low altitude required by the infrared imaging. In such methodology, the aircraft dimensions were determined considering the autopilot characteristics and this is an important aspect of the UAV design.

The work reported in this paper is inserted into the preliminary design phase, where more accurate information has to be used in order to improve the analysis methods used to determine the airplane dimensions, as well as, the relative positions of the different aircraft parts (wing, fuselage and tail). One of the problems verified during the conceptual design phase was the lack of information on low Reynolds number aerodynamic data, required to a small vehicle at low velocity. Such kind of information is very useful to generate the aircraft characteristic curves (CL x α, CL x Cm and the drag polar), which are used to performance, as well as, stability and control calculations.

The objective of this paper is to present aerodynamic data for the influence of flap deflection angle on the characteristic curves of the airfoil chosen to the UAV wing, for low Reynolds number. A wind tunnel is used to determine the aerodynamic coefficients of a two element airfoil model, characterized with a 25% chord ratio flap. A three component balance is used to obtain lift, drag and pitch moment of the airfoil and a special device is used to measure the flap hinge moment. During a specific test the flap deflection angle is fixed at some value and the angle of attack is varied in order to determine the airfoil characteristic curves. A set of tests, for different flap deflection angles were performed, with the objective to obtain the following information: (i) Variation on the lift coefficient for angle of attack equal to zero, (ii) variation of the lift curve inclination ($dCl/d\alpha$), (iii) variation on the angle of attack for $Cl = 0$, (iv) variation of the maximum value of lift coefficient, (v) variation of the drag coefficient, for $Cl = 0$, (vi) variation on the pitch moment coefficient, around the airfoil aerodynamic center. The information generated above is very useful to determine the control derivatives of the airplane developed in this project.

During the design conceptual phase a semi-empirical methodology were used to estimate values to the stability and control derivatives. Such methodology is compared with the experimental results, obtained in tests mentioned above, in order to verify its applicability to a low Reynolds number range. If possible, some methodology adjustments can be done and the new methodology will be very useful in future aircraft development, when other airfoil will be used.

2 EXPERIMENTAL APPARATUS

The measurements were performed in a blower wind tunnel with square test section, characterized by a dimension of 460 mm. The flow velocity ranges from 4 to 30 m/s and the turbulence intensity is 0.5% at the maximum velocity. Along the test section length the cross section area is changed in order to compensate the boundary-layer growth and, as a consequence, to keep a constant static pressure. This area change is performed by filling the test section corners with triangular elements, whose dimension changes along test section length.

Lift, drag and pitch moment of a model are measured with a balance fixed at the test section lateral wall (outside the wind tunnel). Aerodynamic forces and moment on the model are transmitted to the balance through a metal axis. Such balance has a triangular plate used to fix the metal axis originated at the model. The triangular plate is connected to the wind tunnel structure by using three load cells (metal plates, instrumented with four strain gages each, in order to assembly a complete Wheatstone bridge). Two of these load cells are used to make measurement of lift and pitch moment (sensors A and F) and the third one is used to obtain drag force measurements (sensor D). Each load cell is connected to an independent signal conditioner module (amplifier and filter), which allows adjustment of the output voltage considering the data acquisition board characteristics. For the present experiment, the maximum output voltage of each sensor is chosen to be 10 volts, which maximize measurements resolution.

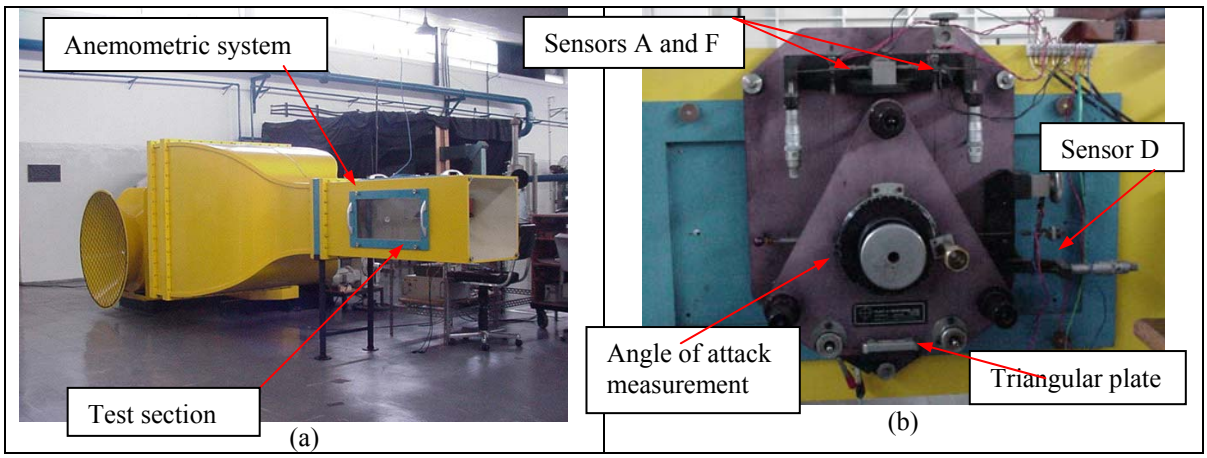

Figure 1. (a) Open circuit wind tunnel and (b) three component aerodynamic balance.

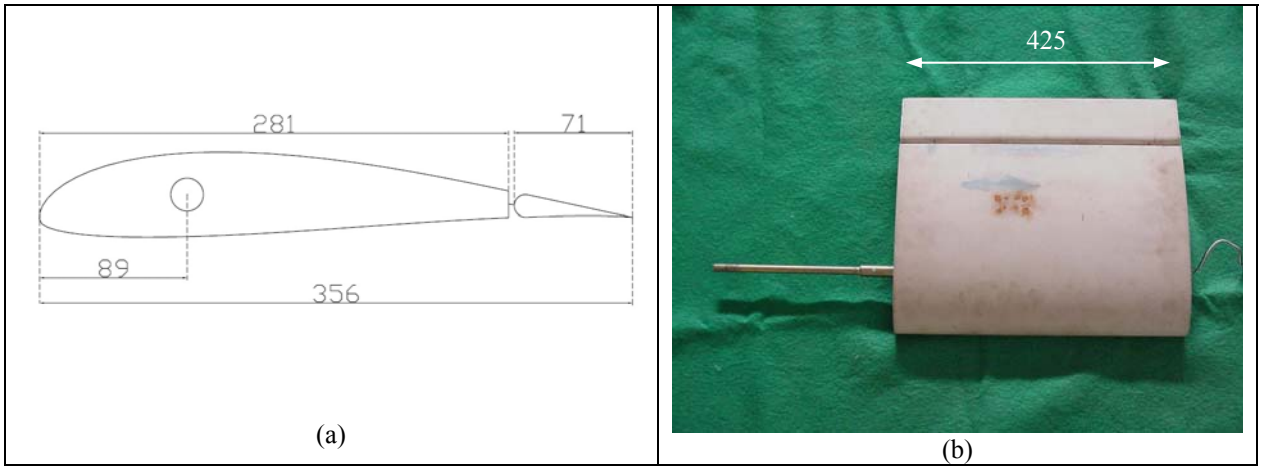

Figure 2. Airfoil and its flap: (a) lateral view and (b) plan view (from the top). Dimensions in mm.

The dynamic and static pressures are measured by using a Pitot tube located at the beginning of the test section (tunnel anemometric system), just after the end of the contraction section, as can be seen in the figure . Pressure transducers are connected to the Pitot tube and a signal conditioner is used to amplify the output voltages before the connection with the data acquisition board.

The model angle of attack is varied manually and its measurement is performed by a rotating device (where the model axis is fixed) divided in 360 equal parts. The uncertainty of ± 0.5 degrees can be considered to this measurement.

The Selig SD7062 airfoil with 20% chord ratio plain flap (see Fig. 2a) was used as a model in the present work. It was manufactured with wood and its main dimensions are: 356 mm total chord, 425 mm spanwise dimension and 71 mm flap chord. The flap is connected to the main airfoil by using four plastic hinges, along the model span, and a gap of 3.5 mm was left between the airfoil two elements. A metal axis, used to connect the model to the balance, was fixed at 89 mm from the airfoil leading edge, as shown in the Fig. 2a.

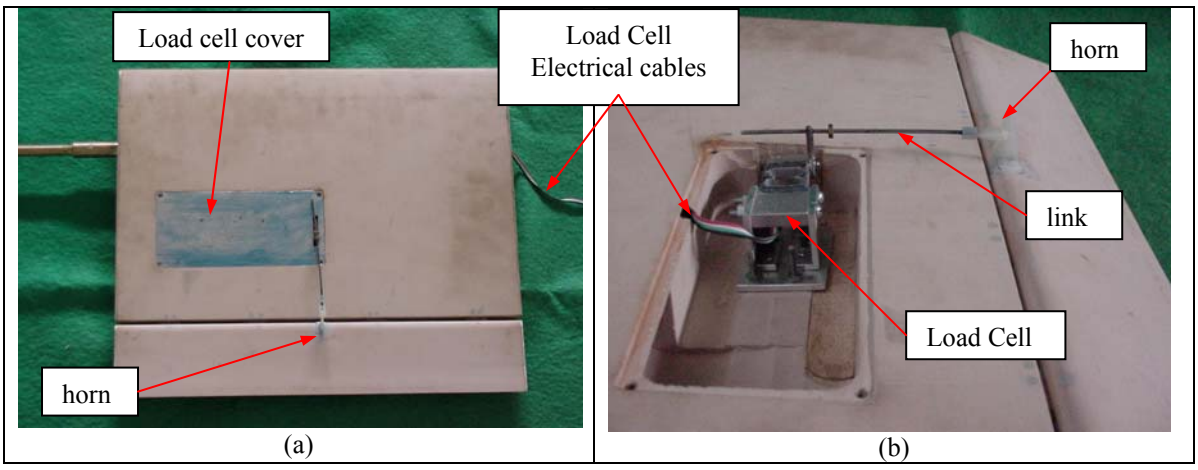

Figure 3. Hinge moment measurement apparatus: (a) lateral view and (b) plan view (from the bottom)

In order to make measurements of the flap hinge moment, a special apparatus was developed. A horn was fixed at the flap leading edge region (see Fig. 3a and b) and it was used to rotate the control surface around the hinges fixed to the main airfoil element. The main idea is to determine the force required to avoid the flap rotation and calculate hinge moment by using the distance from the hinge axis to the force application point. A small load cell, capable to make measurements of forces up to 2 kgf, was inserted inside the main element airfoil (see Fig. 3b) and a metal rod was used to link the load cell to the horn fixed at the airfoil flap, as shown in the Fig. 3b. This load cell is connected to a signal conditioner, through electric cables leaving the model by the extremity opposite to the metal axis used to fix the model to the aerodynamic balance. From the signal conditioner the signal is sent to the data acquisition board. Finally, a metal plate covers the force measurement apparatus (see Fig. 3a) in order to minimize the flow field disturbance, caused by the measurement device.

Once a cambered airfoil was chosen to be used at the UAV's wing, one important task to be performed in the aerodynamic tests is the initial alignment of the angle of attack. First of all, an axis is found parallel to the upper and lower test section walls and it is stamped on the end plates surfaces. Those axes are used to guide the fixation of model drawings, using chord line as a reference. When the airfoil is assembled inside the wind tunnel, the drawings fixed on the two end plates surfaces are used to model alignment. The same drawings are used to establish the initial flap deflection, that is, deflection value when airfoil angle of attack and dynamic pressure are zero. Several lines, originated at the hinge axis and with different angles of flap deflection, are used to this initial deflection angle setup. The initial flap deflection angle is changed manually by using a system with two sows and a screw thread applied to the rod used as the link between the load cell and the horn fixed at the flap surface, as can be seen in the Fig. 3. Finally, it is important to note that the flap deflection angle is changed when wind tunnel is turned on and flap hinge moment cause small configuration distortion, due to the deformation on the load cell and on the rod. Such distortion has to be determined in order to correct the initial flap deflection. This task is performed during the load cell calibration procedure, as will be explained later in this paper.

End plates are used to isolate the wind tunnel boundary layer from the flow over the two dimensional model, in order to minimize three-dimensional flow, which is normally found at the model extremities (see Bearman (1958) and Girardi (1965)). The experimental results reported by Kubo (1989), were used, initially, to define the end plates dimensions. The distance the end plates are fixed from the wind tunnel lateral walls are defined as a function of the boundary layer thickness, determined by Sousa (1993) by using a hot wire anemometer.

After the first experiments with the model installed, a flow field between the two sides of the end plates was observed, generating a longitudinal vortex, whose intensity was increased with the airfoil angle of attack. The cause of such problem is the low pressure at the airfoil upper surface, associated to the flow established from the gap, between the test section wall and the end plate surface, and the region limited by the two end plates. Due to such flow a vortex is generated at the end plate upper edge. A similar vortex (with the same orientation) appears at the end plate lower edge, caused by the high pressure at the airfoil inner surface. As the pressure difference increases with airfoil angle of attack, the longitudinal vortex intensities are incremented. The three-dimensional flow observed over the airfoil span (tufts visualization) is a consequence of the problem discussed above, which has to be minimized in order to determine reliable results for the two-dimensional model under study.

Considering the above paragraph analysis, the three-dimensional behavior along the model span could be minimized by using end plates spanning all the wind tunnel test section height (the airfoil is fixed at the horizontal position) in order to avoid the flow established along the upper and lower edges of the end plates. Due to the area variation along the wind tunnel test section (boundary layer compensation to keep static pressure constant along the test section length) the end plates have trapezoidal shape. Thin rubber strips are fixed along the upper and lower edges of the end plates and such edges are mounted flush to the test section corner surfaces, in order to guarantee a complete sealing between the regions mentioned above and avoid vortex formation.

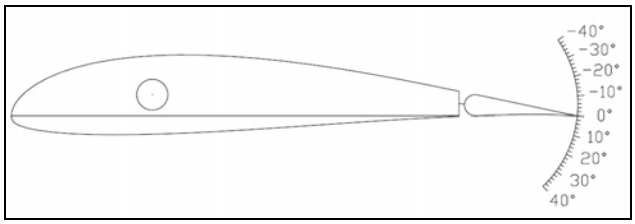

Figure 4. Airfoil main element and its flap drawing

3. EXPERIMENTAL PROCEDURE

In the present work, the following measurements have to be performed: (i) the forces and pitch moment of the complete model configuration, (ii) force required to determine the flap hinge moment and (iii) the dynamic pressure, necessary to obtain the non-dimensional coefficients for lift (C_L), drag (C_D), pitch moment (C_M) and flap hinge moment (C_H). In this paper section, only the experimental procedure established to the calibration of the hinge moment is described. The remaining measurements are described at de Araújo et al (2007).

The hinge moment experimental apparatus is calibrated with the model assembled inside the wind tunnel and fixed at the aerodynamic balance. The main idea is to obtain a correlation between a force applied to the horn fixed to the flap and the load cell output voltage. Such force is the weight of standard masses, transmitted to the horn by a system constituted by a cable and a pulley, similar to that used to the drag sensor calibration. As in the aerodynamic balance, increments and decrements of the standard masses are used to obtain the calibration curve. Due to the flexibility of (i) the load cell, as well as, (ii) the load cell – horn link, the hinge moment applied to the flap results in a flap deflection angle variation. During the calibration procedure, the correlation between the hinge moment and the flap angle variation

is obtained and such calibration curve will be used to correct the initial flap angle, established before wind tunnel is turned on. The flap angle variation is measured through the drawing fixed to one of the end plate surface.

Data generated during calibration procedure, as well as during the experiment are used to determine the uncertainty associated to each aerodynamic coefficient. The uncertainty analysis was made by using the procedure described by Kline and Mcintoch (1953). All the presented uncertainties are associated with a probability of 95% (2σ).

4. ANALYSIS OF RESULTS

The results obtained for the lift coefficient are presented below for some flap deflection angles. Although tests were performed using deflections of 0° up to 26°, with intervals of 2°, only the results for some deflections are shown in order to make easier the visualization of the results. All the presented results for the lift coefficient were corrected to eliminate the blockage effect using the procedure described by Gomes (2005).

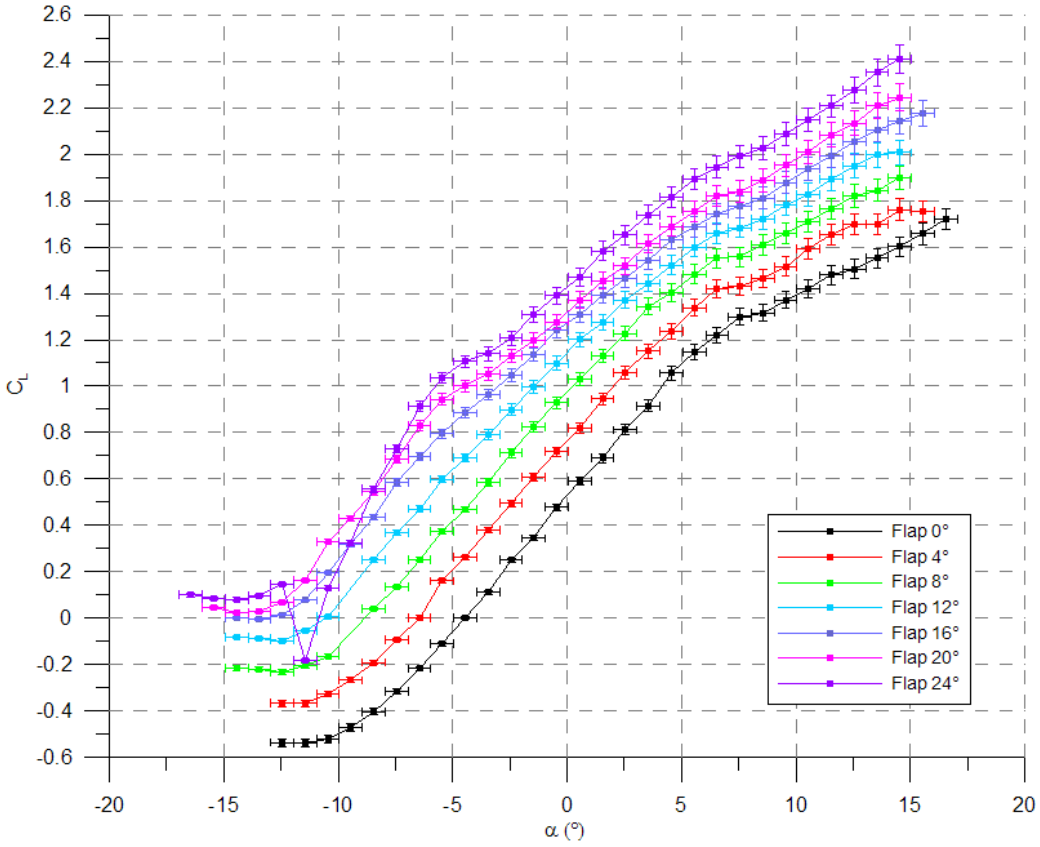

Figure 5. Airfoil lift coefficient for different flap deflection angles. Re = 4 x 10^5

For angles greater than 7 degrees, a separation of the boundary layer was detected at the neighborhood of the endplates. This was visualized using wool tufts, which oscillated at these regions, showing reversal of the flow direction and unsteady flow. The resulting flow is thus three-dimensional, and affects the measured lift coefficient. The stall cannot be determined by the analysis of Figure 5. In fact, even for great angles of attack the boundary layer remained attached at the center of the airfoil model. Thus, the results do not present the expected decrease of the lift coefficient for high angles of attack, due to three-dimensional effects. Consequently, the presented results are valid up to $\alpha = 7°$, and should be disregarded for higher angles.

For a flap deflection of 24 degrees, a different behavior was noted for angles smaller than -8.5°. An intense variation of the lift coefficient was measured between -11.5° and -8.5°. Flow visualization allowed the detection of a separation of the boundary layer at both the upper and lower surfaces of the airfoil. The separation at the upper surface is due to the high adverse pressure gradient at the flap leading edge, and the separation at the lower surface is related to the adverse pressure gradient after the airfoil leading edge. This kind of behavior was also observed for flap deflections of 22° and 26°.

The comparison of the curves in Figure 5 shows the effectiveness of the flap deflection in order to increase the lift coefficient. It can be seen that greater flap angles have higher lift coefficients for each angle of attack, which is in agreement with the expected results by potential theory.

However, it can also be seen that there is a smaller increase of the lift coefficient by a greater flap deflection. A wool tuft allowed flow visualization at the flap surface. It could be seen for an angle of attack equal to -2.5° that with the flap at 16° there was separation of the boundary layer at the trailing edge, and with the flap at 20° there was separation over the whole surface of the flap. This separation reduces the lift of the airfoil.

To allow a better comprehension of the variation of the lift coefficient with flap deflection, the values of C_L at $\alpha = 0.5°$ for each flap deflection are presented in the figure below, as well as the predicted values using the method described by Roskam (2000) and the numerical results generated with XFOIL, a panel method code with boundary layer corrections developed by Drela (2007). The values of C_L with zero flap deflection were equalled to provide a comparison between the variations of the moment coefficient.

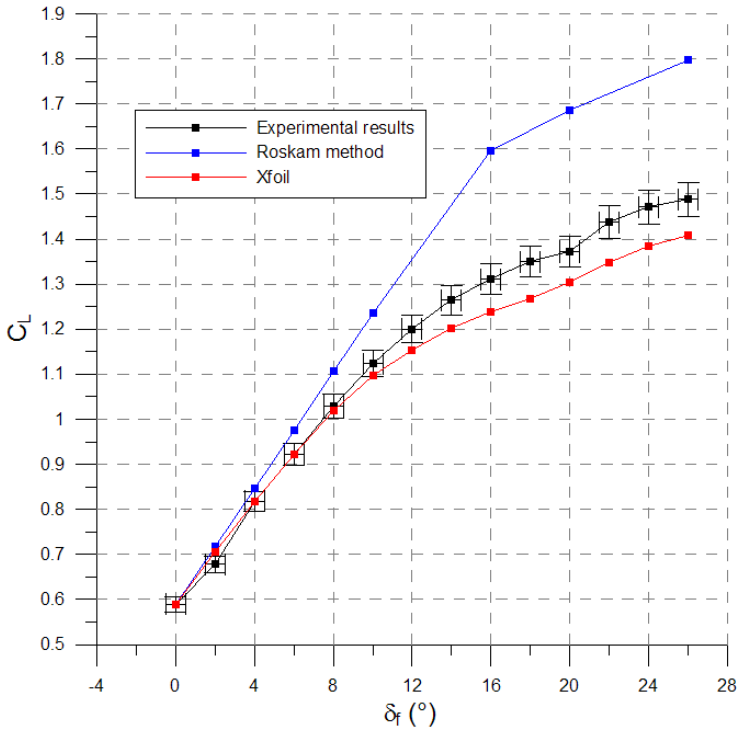

Figure 6. Lift coefficient at $\alpha = 0.5°$ for the tested flap deflections. Re = 4 x 10^5

The observation of Figure 6 shows that greater flap deflections provide higher lift coefficients. At first, the rise of the lift is linear, and for higher deflections the graph shows a non-linear behavior. This can be seen for the experimental results and for the calculated values.

It is important to remark that the procedures described at Roskam (2000) are valid for Reynolds numbers greater than the typical ones for UAVs. The comparison presented in Figure 6 shows that for a Reynolds number of 4 x 10^5 the non-linear behavior begins for a deflection of about 8°, and the predicted values show the same behavior beginning at a deflection of 10°. It is also seen that the experimental lift coefficients become much lower than the predicted values for a higher Reynolds number.

The variation of lift coefficient with flap deflection is of great importance for the determination of the control derivatives of an aircraft, related to the ailerons, the elevator or the rudder deflection.

The results for the drag coefficient are shown in the figure below. Again, only the results for some flap deflections were plotted to allow a clearer visualization. These results are presented without wind tunnel corrections, which were not done because the correction procedure employed for the results is based on potential theory and does not allow a drag analysis.

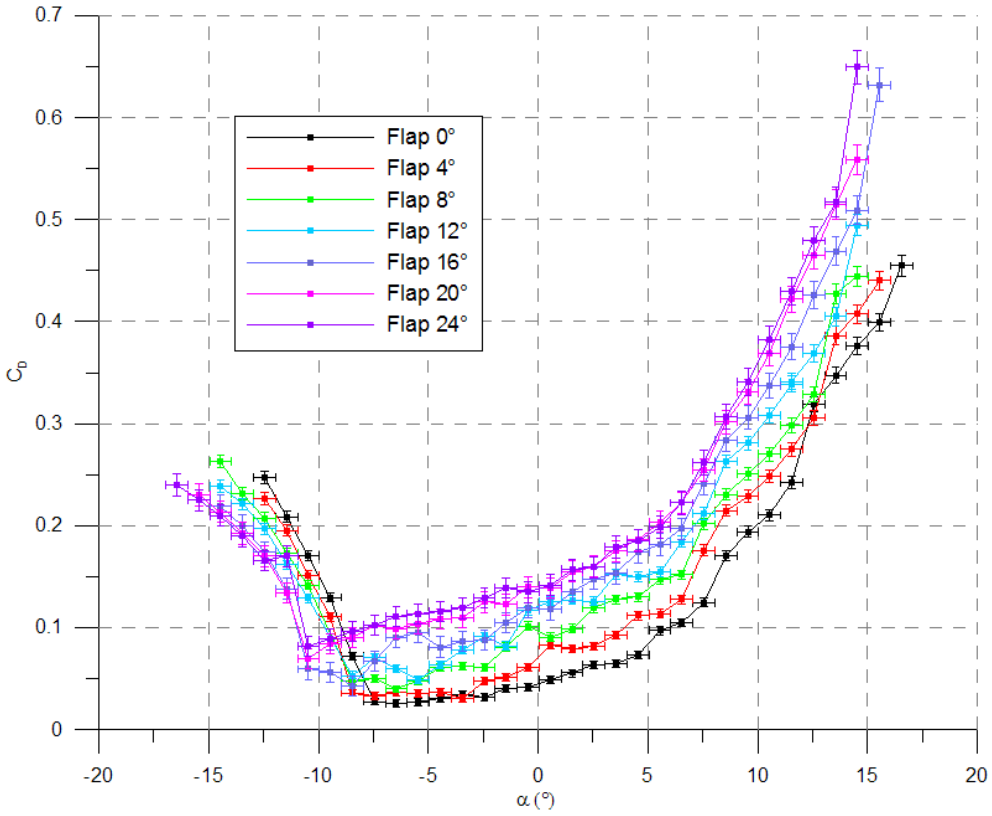

Figure 7. Airfoil drag coefficient for different flap deflection angles

The figure above show a rise in the drag for most of the angles of attack, with the exception of some negative angles, where there are some differences related to the angle of negative stall. It is possible to see with Figure 5 that the negative stall occurs for lower (more negative) angles of attack for the higher flap deflections. The drag rise associated with boundary layer separation is responsible for the differences between the curves for negative angles.

For the remaining angles of attack, the differences in drag are related to the boundary layer separation at the upper flap surface. For small angles of attack the drag values for the different flap deflections are closer, and the differences become greater as the boundary layer starts to separate at the flap surface.

However, a wind tunnel correction for the drag would be useful to analyze the data more accurately, since different flap deflections are related to different block ratios at the test section, and the block ratio changes the drag coefficient of a body in a wind tunnel test.

It is possible that the oscillations observed in the drag coefficient were caused by the deformation of the tape used to seal the gap between the airfoil and the flap. Since this tape is very flexible, the shape of the body at this region may be modified for each angle of attack, changing the characteristics of the boundary layer separation at the flap. However, the determination of the exact reason for these oscillations requires further experiments.

The values for the moment coefficient at the airfoil's quarter chord are presented below. As in the graphs of lift and drag coefficient, some of the tested flap deflections were omitted to allow a clearer visualization.

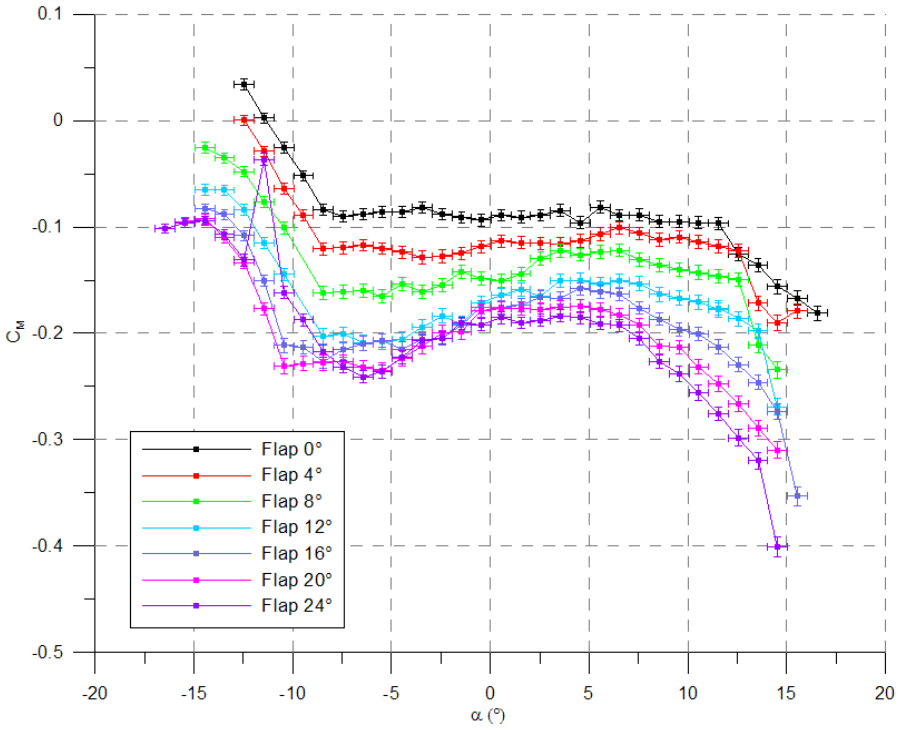

Figure 8. Airfoil moment coefficient at the quarter chord for different flap deflection angles. Re = 4 x 10^5.

Figure 8 shows an expected behavior for the moment coefficient, which becomes almost constant for the linear range of angles of attack, showing that the position of the aerodynamic center is close to that point. As boundary layer separation starts, there is a change in the moment coefficient, which becomes more negative if the separation is at the upper surface of the airfoil, and becomes less negative it the separation is at the lower surface.

The results presented in the figure above show again the lost of efficiency as the flap deflection is increased. Since high flap deflections cause the separation of the boundary layer at the upper surface of the flap, the generated lift at this region is smaller than the lift of an attached flow configuration. Since the lift generated at the flap contributes to a negative moment, a smaller lift at the flap leads to a less negative moment coefficient.

In order to allow a comparison of the moment coefficients for the different flap deflections, a graph is shown in the next figure. Numerical results generated with Xfoil are also presented. The values of C_M with zero flap deflection were equalled to provide a comparison between the variations of the moment coefficient.

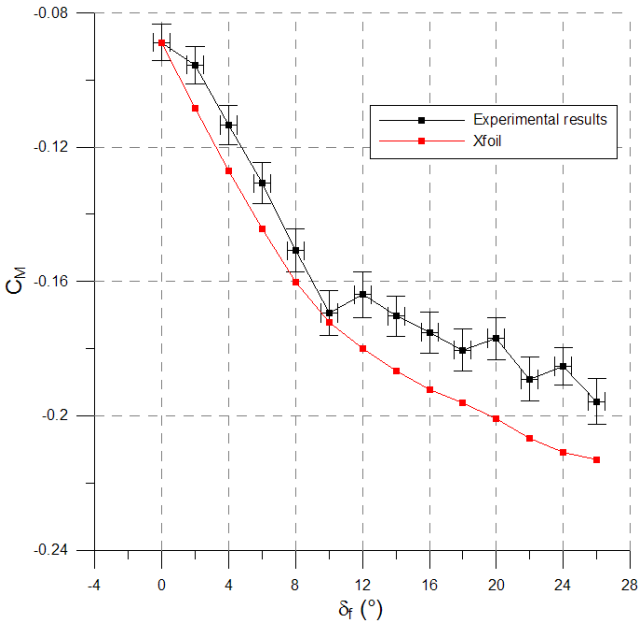

Figure 9. Moment coefficient at the quarter chord for α = 0.5° for the tested flap deflections. Re = 4 x 10^5

It is possible to see that the flap deflection is related to more negative moment coefficients for a fixed angle of attack. This relation at first is linear, and non-linear effects become significant starting with a deflection angle of 10 degrees. Figure 9 shows that non-linear effects can be perceived in the lift coefficient at this deflection angle. Both effects are related to the loss of lift at the flap due to separation of the boundary layer. This loss of lift decreases the total lift coefficient, and also causes the moment coefficient to be less negative than it would be if the boundary layer remained attached to the surface, since the lift at the flap region has a negative contribution for the moment coefficient.

The numerical results obtained with Xfoil capture well the behavior of the moment coefficient with flap deflection, with maximum deviation of about 10% of the experimental value for the results shown in Figure 9. The differences may be due to the modeling of the flap by the software, which does not include a hinge, as shown in the figure below, which represents the SD7062 profile with 20 degrees of flap deflection.

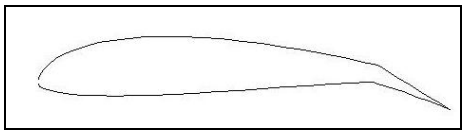

Figure 10. Geometry used by Xfoil to simulate an airfoil with flap

The experimental results for the hinge moment coefficient are shown in the following figure. The results are not corrected for blockage effects. Although the method of correction for C_L and C_M could be used to correct the hinge moment coefficient, this is still not developed up to this point, being a work to be done in the near future.

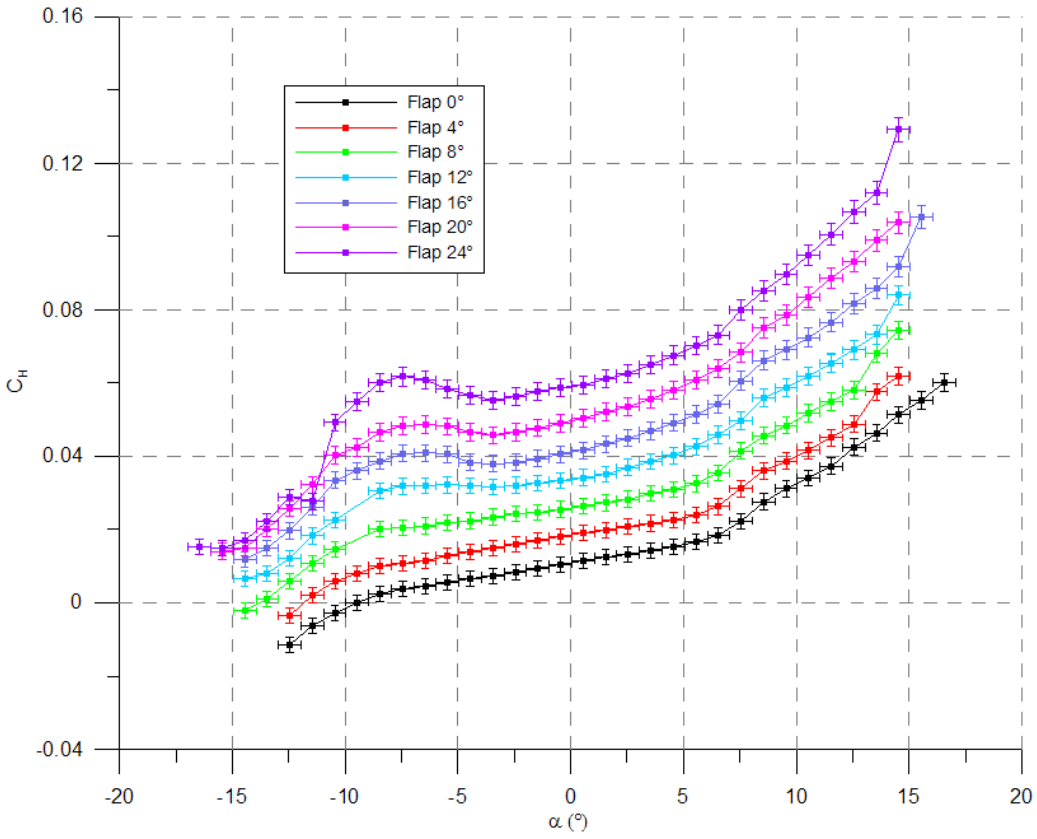

Figure 11. Hinge moment coefficient for different flap deflection angles. Re = 4 x 10^5.

The results presented in Figure 11 show that the hinge moment coefficient becomes higher as the angle of attack is increased, and also as the flap deflection is increased. It can also be seen that the curves do not become closer for high flap deflections, showing that boundary layer separation increases the hinge moment. This may seem to be in contrast with the loss of lift at the flap when separation occurs. However, the high pressure drag at the flap has an important contribution to increase the hinge moment coefficient. This effect can be seen at any of the curves by noticing that for high angles of attack the slope of the curve becomes greater; this shows that the boundary layer separation at the flap increases the value of the hinge moment.

This shows that the evaluation of pressure drag due to boundary layer separation is of great importance in the determination of the hinge moment coefficient, specially for high angles of attack and flap deflections. Since those are the most critical values for the specification of the mechanism to move the flap, boundary layer separation must be accounted in design phases. The hinge moments shown here can be interpreted also as the necessary moments to move an aileron, an elevator or a rudder.

5. FINAL REMARKS

The experimental results presented in this work were used at the preliminary design phase of an Unmanned Aerial Vehicle, and allowed the creation of an aerodynamics database for flight dynamics calculations. Although at the beginning of the design simpler methods were used to determine the aerodynamic characteristics of the aircraft, the following phases require more accurate data, which can be obtained by wind tunnel tests.

The results for the lift and the moment coefficient show that non-linear effects must be accounted for the calculations related to high flap deflections. The experimental results are in good agreement with those predicted by Xfoil. The method developed by Roskam (2000) is less accurate for the present Reynolds number.

From the data presented in this paper, a new design technique can be developed to allow a more accurate determination of the aerodynamic characteristics of wings with control surfaces. This work will be developed soon in order to create a tool for efficient design of UAVs.

6. ACKNOWLEDGEMENTS

To the Financiadora de Estudos e Projetos (FINEP), for supporting part of the resources used to the Unmanned Aerial Vehicle development (protocolo 243/2004) and to the Centro de Estudos de Sistemas Avançados do Recife (CESAR), to the partnership in this project. To the staff of the Prof. K.L. Feng Aeronautical Engineering Laboratory: Carlos Guedes Neto, Luis Zambrano Lara, Vitor Valentim Betti and Mario Correia.

7. REFERENCES

Bearman, P.W. (1965): Investigation of the flow behind a two-dimensional model with a blunt trailing edge and fitted with splitter plates. *J. Fluid Mech*., Vol. 28, pp. 241-255.

de Araújo, T.B., Girardi, R.M. and Cavalieri, A.V.G., (2007), "Experimental Determination of the Wing Airfoil Aerodynamic Characteristics used at ITA's Unmanned Aerial Vehicle (UAV)".19th International Congress of Mechanical Engineering, Brasília, Nov. 5-9.

Drela, M., "XFOIL Subsonic Airfoil Development System". 28 Feb. 2007, <http://web.mit.edu/drela/Public/web/xfoil/>

Girardi, R.M. e Rizzi, P., (2005a), "Análise do tipo da aeronave mais adaptada para a inspeção de linhas de transmissão", Relatório de Trabalho, CESAR/ITA, 27 de junho.

Girardi, R.M. e Rizzi, P., (2005b), "Seleção da alternativa mais promissora para prova de conceito, através da construção e testes em vôo", Relatório de Trabalho, CESAR/ITA, 27 de junho.

Girardi, R.M. e Rizzi, P., (2006), "Desenvolvimento de Metodologia para Projeto Conceitual de um Veículo Aéreo Não Tripulado (VANT), Usado para Inspeção de Linhas de Transmissão de Energia Elétrica", Anais do Congresso Nacional de Engenharia Mecânica (CONEM), Recife, Pe.

Girardi, R.M. e Rizzi, P., (2006), "Projeto Conceitual de um Veículo Aéreo Não tripulado, Usado para Inspeção de Linhas de Transmissão de Energia Elétrica". Anais do 11° Encontro Nacional de Ciências e Engenharia Térmicas (ENCIT 2006), Curitiba, Dez. 5-8.

Gomes, C.D.A.N., (2005), "Avaliação da Razão de Bloqueio Bi-Dimensional Utilizando Método dos Painéis". Trabalho de Conclusão de Curso (Graduação) – Instituto Tecnológico de Aeronáutica, São José dos Campos.

Kline, S.J. and McClintock, F. A. (1953): Describing uncertainties in single-sample experiments. *Mechanical Eng*., pp. 3-8.

Kubo,Y. et all.(1989): Effects of end plates and blockage of structural members on drag forces. *J. Wind Eng. Ind. Aerodynamics*, vol.32, pp.329-342.

Rae, W.H. and Pope, A, (1984), *Low speed wind tunnel testing*. Second edition, John Wiley & Sons, USA.

Raymer, D.P., (1999), "Aircraft design: a conceptual approach", AIAA Education Series, AIAA, Washington DC.

Roskam, J., (2000-2003), "Airplane design", parts I-VIII, Dar Corporation, Lawrence, Kansas, USA.

Sousa, F.L., (1993), "Influência da razão de bloqueio no escoamento plano sobre corpos rombudos", Master Thesis, Instituto Tecnológico de Aeronáutica (ITA), S.J.Campos, SP.

8. RESPONSIBILITY NOTICE

The authors are the only responsible for the printed material included in this paper.